Editors' Suggestion

Proximity-Induced Gap Opening by Twisted Plumbene in Epitaxial Graphene

Chitran Ghosal, Markus Gruschwitz, Julian Koch, Sibylle Gemming, and Christoph Tegenkamp*
Institut für Physik,Technische Universität Chemnitz, Reichenhainer Straße 70, 09126 Chemnitz, Germany

(Received 10 April 2022; accepted 17 August 2022; published 8 September 2022)

Besides graphene, further honeycomb 2D structures were successfully synthesized on various surfaces. However, almost flat plumbene hosting topologically protected edge states could not yet be realized. In this Letter, we investigated the intercalation of Pb on buffer layers on SiC(0001). Thereby, suspended and charge neutral graphene emerged, and the intercalated Pb formed plumbene honeycomb lattices, which are rotated by $\pm 7.5°$ with respect to graphene. Along with this twist, a proximity-induced modulation of the hopping parameter in graphene opens a band gap of around 30 meV at the Fermi energy, giving rise to a metal-insulator transition. Moreover, the edges of the intercalated plumbene layers revealed edge states within the gap of the conduction bands at around 1 eV as expected for charge neutral plumbene.

DOI: 10.1103/PhysRevLett.129.116802

Stimulated by the intriguing physics demonstrated with graphene [1], intense research on the synthesis of further monoelemental 2D materials, e.g., silicene, germanene, borophene, bismuthene, etc. on various surfaces was conducted [2–6]. In the case of epitaxial graphene (EG), both metallic and insulating surfaces were shown to be suitable templates for the growth of a flat and suspended 2D Dirac material [7,8]. Recently, with the consideration of twisted multilayer structures of graphene, revealing superconducting and so-called Moiré nematic phases, a new direction of research seems to have been established [9–11].

Compared with graphene, the other monoelemental 2D materials of group 14 elements are less flexible; thus the surfaces play an important role. As a matter of fact, these systems were grown on metallic substrates, which must compensate for the limited hybridization capability of the group 14 atoms. For instance, silicene was successfully grown on Ag(110) and Ag(111) surfaces [12,13]. The mixed sp^2/sp^3 hybridization comes along with buckling, and a more pronounced interaction with the substrate was reported for Pt(111) revealing a reconstruction rather than a Moiré structure [5]. For germanene on Pt(111) even a strong buckling is found [3], and some of the relativistic signatures of the 2D adlayer can be restored by using more complex supports, e.g., Ge_2Pt crystals [14]. Stanene grown on Bi_2Te_3 was the first candidate of these group 14 elements considered as a 2D topological insulator [15]. Since then, the last cousin of graphene, i.e., plumbene, started to come into the focus of research and, again, the use of $Pd_{1-x}Pb_x(111)$ alloys or magnetic Fe layers on Ir(111) were mandatory to stabilize the structure of plumbene [16,17].

Because of the higher intrinsic spin-orbit coupling (SOC), the high-Z 2D layers are expected to host signatures of a quantum spin Hall insulator (QSHI). The Dirac-point degeneracy in honeycomb structures of group 14 elements is lifted by SOC, and the appearance of edge states is a hallmark for this class of material [18]. Moreover, adlayers of elements with different valence states were successfully used to form QSHI systems, e.g., by forming bonds to the SiC(0001) on purpose, giving insight into a universal concept to realize high temperature QSH systems, e.g., in case of bismuthene [4], and use triangular lattices instead of honeycomb symmetries, as recently shown for indenene on SiC(0001) [19].

In this context, the stabilization of a flat and quasisuspended honeycomb lattice is mandatory for Pb [20]. The $6p_z$ states of hybridized Pb form a Dirac cone at the K point; however, the high intrinsic SOC opens a band gap of 400 meV at the Fermi energy [20–22]. Also, the degeneracy at E_F of the s and $p_{x,y}$ states at Γ is lifted, and due to the avoided crossing of the s and p_z states along the ΓK direction a second gap at around $+1.5$ eV shows up. The gap at the Fermi energy between the valence and conduction bands is topologically trivial, while an inverted gap is formed between the first and second conduction band. For zigzag-plumbene ribbons topologically protected edge states were predicted at $+1.2$ eV [16,20]. For Pb the sp^3 hybridization is preferred; thus plumbene tends to be buckled [21,23]. This is contrary, for almost flat plumbene, a band inversion in the valence bands is expected with topological insulator (TI)-edge states; thus, charge neutral plumbene can be a quantum spin Hall (QSH) system [16].

EG on SiC(0001) is perfectly suited to realize plumbene. Graphene grows epitaxially on SiC(0001), and its comensurability is underlined by the diffraction spots of the $(6\sqrt{3} \times 6\sqrt{3})$ lattice ($6\sqrt{3}$ hereafter). The lattice constant of plumbene is approximately twice as large as of graphene, i.e., plumbene is also commensurate to the substrate. Intercalation experiments on buffer layer (BL) structures

on SiC(0001) have been performed for many years. In those experiments, often the bonds of the BL to the SiC substrate are saturated by the intercalates, such that quasifreestanding graphene is formed. Depending on the elements, almost charge neutral EG as well as extremely doped EG monolayers were fabricated [24,25]. Using the concept of intercalation to form long-range ordered 2D interface layers might be an interesting concept to generate proximal 2D heterobilayer systems.

In this Letter, we report on the intercalation of Pb on BL/SiC. High resolution STM measurements at various tunneling conditions allow for an effective subsurface resolution providing evidence for the formation of plumbene in between SiC and EG. The details of the electronic corrugations are perfectly resembled by considering two plumbene lattices rotated by $\pm 7.5°$ with respect to EG. The local spectroscopy at low temperature shows the opening of a gap at the Fermi energy, which is in line with a metal to insulator transition found by electronic transport experiments [26] and is explained by modulation of the energy landscape due to the proximity of twisted plumbene.

Intercalation of Pb was obtained by subsequent deposition of Pb multilayers at room temperature followed by postannealing to 770 K for 5 min. The intercalation process occurs via defects within the BL, and the rate of intercalation can be increased by mild Ar sputtering of the surface before intercalation [26]. The structures were analyzed by high resolution low energy electron diffraction (SPALEED) and scanning tunneling microscopy (STM) using KOH-etched W tips. Local tunneling spectroscopy (STS) was conducted with a lock-in amplifier at 800 Hz with a modulation voltage of 10 meV. The local density of electronic states close to E_F was obtained by π-orbital tight-binding calculations in the $6\sqrt{3}$ supercell. The electrostatic potential of a free-standing plumbene unit cell was obtained by full density-functional calculations [27] following the computational settings of Ref. [16] and employed to modify the on site terms of the tight-binding model to include the proximity of graphene to a 7.5° rotated plumbene layer.

Figure 1(a) shows a STM image of the intercalated phases showing the characteristic stripe formation. The average widths of the stripes of around 2.3 nm, present in three different domains, is nicely captured by the new diffraction spots seen around all integer spots in SPALEED [cf. Fig. 1(b), enlargement of the (00) spot]. From the combined x-ray photoelectron study and STM analysis we concluded that by intercalation a 2-level Pb system is formed [26]. Since the lattice constant of SiC(0001) is considerably lower by almost 20% compared with Si(111), the finite widths of the stripes might be induced by lateral compressive strain [28,29], forming nanostripes of Pb layers.

From the high resolution STM images shown in Figs. 1(c) and 1(d) taken at $V = -400$ mV bias voltage

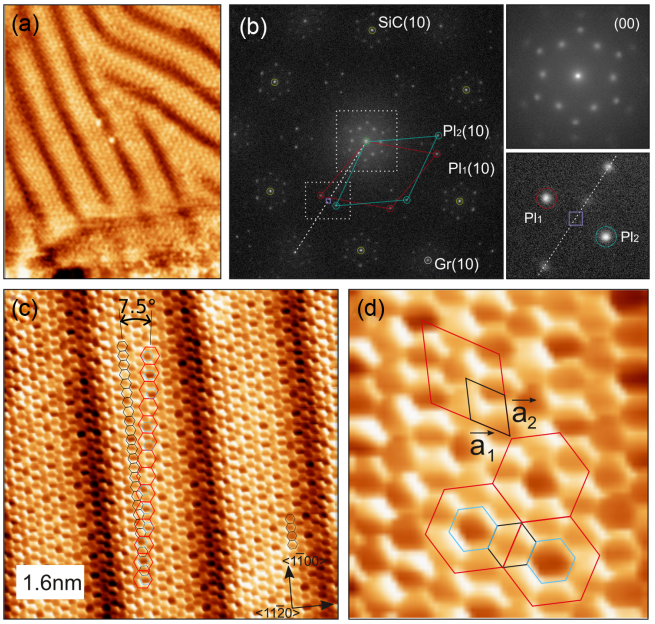

FIG. 1. (a) Large scale STM image (17×22 nm^2, 4 K) showing the formation of stripes upon Pb intercalation. (b) SPALEED image ($E = 168$ eV, 300 K) with close-ups of the (00) region (top) and $6\sqrt{3}$ area. (c) High resolution STM image ($V = -400$ meV, $I = 10$ pA). (d) Enlargement of (c) showing locally an alternating intensity modulation of graphene. This tiling is seen best when the hexagons of plumbene (red) and graphene (blue) are centered. Applying this scheme on a larger scale [see (c)] directly reveals the twist of the two lattices.

it is obvious that a graphene honeycomb lattice is formed upon intercalation and that these Pb-induced stripes are formed along the zigzag direction of graphene. Closer inspection of the STM image shows that on a local scale every second graphene honeycomb cell (marked in blue) appears darker compared with others and is shown in greater detail in Fig. 1(d). This (2×2) reconstruction on the graphene lattice is indicated by red hexagons and a lattice constant of $a_{\mathrm{Pl}} = 4.9$ Å, close to that of plumbene.

However, this $\times 2$ periodicity is seen only on a local scale. In case of a long-range order, we would expect to see half-order diffraction peaks along the $\langle 11\bar{2}1 \rangle$ directions in our SPALEED experiment, indicated by the (violet) square box in Fig. 1(b). Instead, the spots denoted with Pl_1 and Pl_2 become more intense and denote the first order diffraction spots of two twisted plumbene layers. Interestingly, the positions of these peaks coincide with those of the $6\sqrt{3}$ of the former BL structure; thus the plumbene lattice is rotated by $\pm 7.5°$ with respect to graphene. Apparently, the adsorption sites of the intercalates are triggered by the interface bonds of the BL with the SiC(0001) substrate. This rotation in between the topmost layers is obvious also on the large scale STM image in Fig. 1(c). Assuming that the largest change in contrast of a graphene hexagon is obtained for a centric alignment with respect to plumbene,

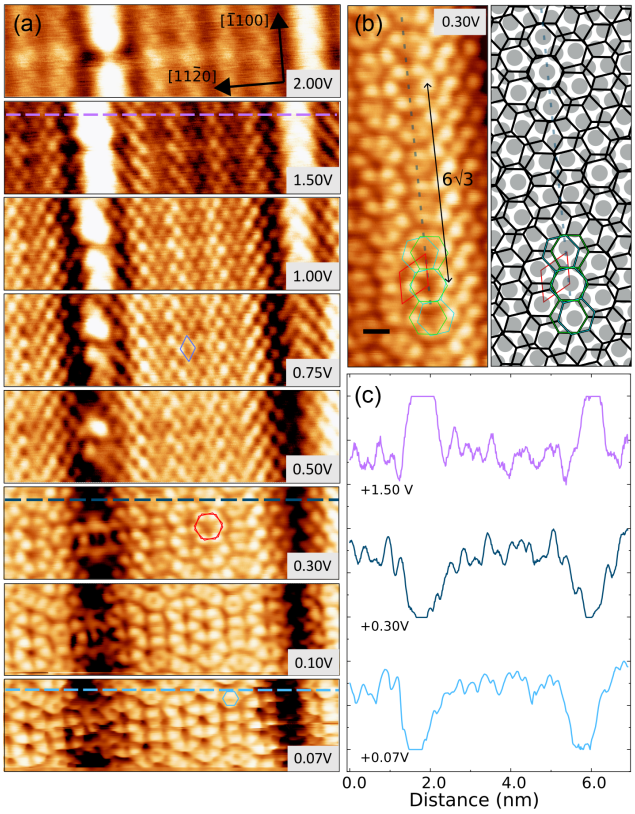

FIG. 2. (a) Sequence of STM images of the same area at different tunneling voltages (I = 25 pA). (b) Extended STM image taken at 0.3 V showing mainly signatures of the rotated plumbene lattices on SiC. (c) Line scans across the nanostripe at three voltages. The unit cells of SiC, graphene and the plumbene lattice are indicated by rhombs and hexagons (blue and red), respectively.

the tiling sequence is also rotated by ±7.5°. The $6\sqrt{3}$ unit cell contains 13 graphene unit cells. In order to account for this odd number of units, the plumbene lattices are rotated, and the first order diffraction spots coincide with the spots of the $6\sqrt{3}$ lattice. The superposition of two oppositely rotated plumbene lattices by ±7.5° in fact aligns with the former $6\sqrt{3}$ symmetry [cf. also Figs. 2(b) and 3(b)]. Besides, as a result of high temperature treatment, partial deintercalation may have taken place, and the Moiré of a suspended graphene layer with SiC(0001) after homogeneous intercalation of a monolayer should also provide the $6\sqrt{3}$ reconstruction spots known from EG/SiC(0001) [30].

Recently, a strained Pb(111) monolayer phase commensurate with a (2×2) SiC lattice was proposed [31]. However, this structure is not compatible with our low energy electron diffraction (LEED) pattern and estimation of intercalated Pb coverage [26] and cannot explain the tiling shown in Fig. 1.

In order to gain insight into the different lattices, we performed bias voltage dependent STM images of the same area. This area in Fig. 2(a) shows a 4.3 nm wide strip with two trenches, one of which also shows a defect for better orientation. In the regime of the unoccupied states, characteristic changes in the structure become apparent: at +1.5 eV above E_F atomic-sized features become visible in STM while the intensity modulation, which is more obvious at even higher tunneling conditions, is visible in between the trenches. In fact, at the positions of these trenches an extremely high transmission is observed, which we discuss in more detail below. However, in the presence of defects, this phase is pinned down to 0.75 eV. At this tunneling condition, the structure of the stripe reveals a (1×1) structure of the SiC(0001) surface.

For tunneling conditions below +0.4 V entirely new motifs become apparent. Most obvious are larger hexagonal structures (red), which we introduced already in the context of Fig. 1(d) and which reveal locally the plumbene lattice. The model proposed in Fig. 1(b) resembles most of

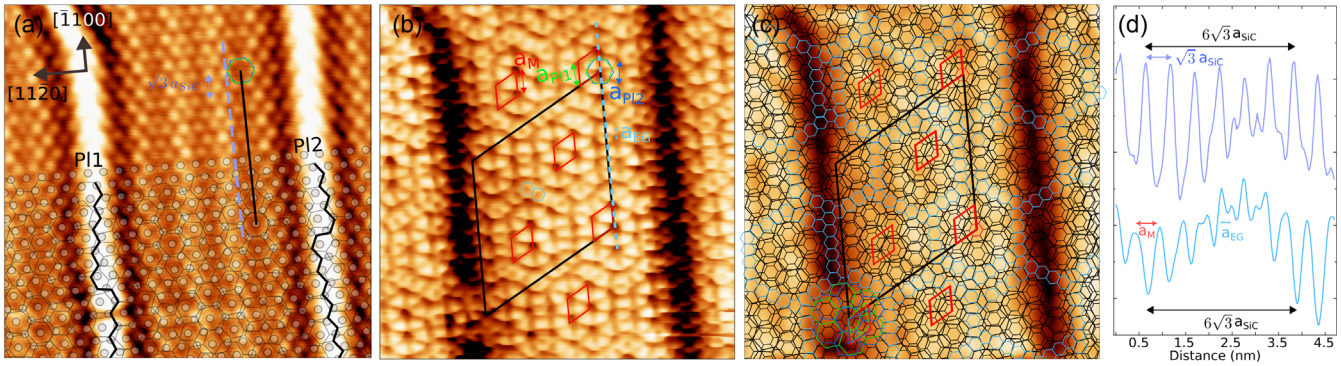

FIG. 3. (a) STM image (7×7 nm^2) taken at +1 V showing the SiC lattice (small circles) and intensity modulations from the plumbene lattice (hexagon). The modulation along the $\langle 1\bar{1}00 \rangle$ direction is indicted by the black line and follows the former $6\sqrt{3}$ symmetry of the BL [(cf. Fig. 2(b)]. The chiral zigzag type edges of the two plumbene lattices (Pl1, Pl2) are marked by thick lines, respectively. (b) and (c) The same area taken at +70 mV. The $6\sqrt{3}$ plumbene unit cells and the graphene honeycombs are shown by black and red rhombs and blue hexagons, respectively. In (c) the graphene lattice (blue hexagons) becomes apparent in "transparent" areas. (d) Line scans taken along the dashed lines in (a) (top) and (b).

the fine structure and commensurability with the $6\sqrt{3}$ structure. By further lowering the bias voltage to 70 mV, the honeycomb lattice of graphene also becomes obvious.

A detailed model of the entire heterostructure is presented in Fig. 3. Figure 3(a) shows an extended image taken at +1 V bias voltage. The bright protrusions coincide perfectly with the (1×1) lattice of the SiC surface, i.e., at these tunneling conditions the intercalated Pb and graphene are electronically transparent. Along the $\langle 1\bar{1}00 \rangle$ direction, some of the protrusions appear even more intense. These spots with a distance of $\sqrt{3}a_{\mathrm{SiC}}$ [cf. Fig. 3(d)], which is close to the lattice constant of plumbene, might therefore resemble a Pb induced modulation. In fact, the intensity of the (1×1) lattice is modulated, and identical motifs, indicated by the hexagons, appear in distances of the $6\sqrt{3}a_{\mathrm{SiC}}$. The position of the high intensity feature at this bias voltage condition coincides with the zigzag directions of each of the two plumbene lattices (thick lines). Figures 3(b) and 3(c) show the same area, but taken at 70 mV. The most apparent features are flowerlike structures, which can be mimicked by overlapping two twisted plumbene lattices and one graphene lattice. According to our LEED analysis, the two plumbene lattices are rotated by ±7.5° with respect to EG. Close inspection of the model reveals that the honeycomb structure of graphene is visible (indicated by blue-colored hexagons), where the honeycomb structure of plumbene below is not interfering with the graphene lattice. At the other sites, the honeycomb structure of plumbene is dominating or modulating the transmission of the electrons. The most noticeable places are marked with unit cells and larger (black) hexagons. This Moiré effect reveals a quasihexagonal structure. The diameter of this quasihexagon [cf. with dotted hexagon in Fig. 3(c)] is around 22 Å and matches nicely with the average widths of the majority Pb stripes shown in Fig. 1. Contrary to previous studies [31,32], our detailed bias dependent analysis supports the formation of Pb multilayers at the interface.

The dI/dV spectra are shown in Fig. 4. The spectrum taken at the ℓN_2 temperature shows the characteristic v shape of the density of states of charge neutral graphene with respect to the Dirac point, in agreement with photoelectron emission experiments [26]. At low temperatures, the spectrum changes completely. Electronic gaps of $E_{g,\mathrm{EG}} \approx 30$ meV and $E_{g,\mathrm{Pb}} \approx 300$ meV show up. These gap sizes are different compared with those reported for suspended graphene, showing an inelastic tunneling gap of around 130 meV [33]. The lines in Fig. 4(a) indicate the voltages, where mainly the SiC, the plumbene, and the graphene lattices were seen (cf. Fig. 2). Most obvious are the shoulders at around 100 meV and 200 meV, which host states originating from graphene and plumbene, respectively. The splitting of $E_{g,\mathrm{Pb}} \approx 300$ meV, measured in between the shoulders, where the plumbene lattice is mostly seen, resembles nicely the spin-orbit gap at the K point of plumbene [20–22].

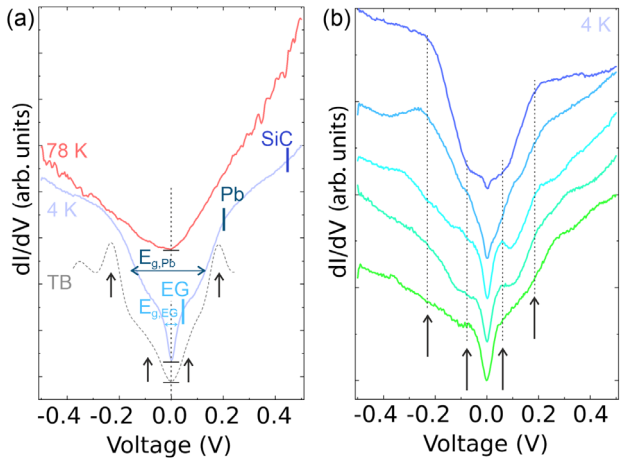

FIG. 4. (a) Spatially averaged dI/dV spectra taken at $T = 78$ K and $T = 4$ K. The vertical lines mark characteristic voltages, where the graphene, plumbene, and (1×1) interface structures were seen (cf. Fig. 2). $E_{g,\mathrm{Pb}}$ and $E_{g,\mathrm{EG}}$ indicate electronic gaps, which originate from plumbene and graphene, respectively. The dashed curve shows the DOS obtained from the tight-binding (TB) calculation. The curve is broadened by convolution with a Gaussian function of 0.1 eV. (b) dI/dV spectra taken at various positions ($T = 4$ K, set point −0.5 V, 25 pA). The dashed lines highlight the characteristic intensity shoulders of the TB curve in (a). All spectra are shifted for better visibility.

The smaller gap is assigned to graphene and is of different origin. As a result of the rotation of the plumbene layers with respect to EG we assume a modulation of the on site elements in graphene. For comparison, Fig. 4(a) also shows the density of states obtained from the tight-binding calculations of the graphene sheet in the electrostatic potential at the van der Waals distance to a 7.5° rotated plumbene layer. The proximity to the plumbene layer induces a symmetry break, which leads to the opening of a gap around the Fermi energy and, secondly, to a decreased band dispersion reflected by shoulders at the band edges and two more prominent signals at ±200 meV from E_F, next to contributions from the plumbene states as mentioned above. These findings reflect very well the experimental features; this indicates that the graphene layer is electrically neutral and undergoes only minor perturbations by the proximity to plumbene. The band gap of 30 meV is in excellent agreement with *in situ* surface transport measurements, where we found a metal-insulator transition at $T \approx 60$ K [26]. In Fig. 4(b) we show low temperature dI/dV curves measured at various ribbons and positions revealing variations at the voltages marked with arrows. Following the tight-binding model, the gap features and shoulders result from the modulation of the on site parameters and backfolding of the band structure due to the Moiré structure. Therefore, the variations in Fig. 4(b) indicate local variations of the interlayer distance and deviations of the twist angle.

The tight-binding calculation for graphene with modulated on site energies is able to reproduce our experiment. Therefore, the coupling in between the graphene and plumbene is weak. Compared with Pb intercalation on graphene/Ir(111) [34], we conclude in our case that the distance is larger so that effective magnetic field effects due to the spin-orbit coupling in Pb seem to play a minor role. Such larger distances are also much more easily subject to height fluctuations mentioned in the context of Fig. 4(b).

So far, we have not addressed the extremely high intensities, seen between +1 V and +2 V voltage biases in the rims of the nanostripes [cf. Fig. 2(c)]. According to our model, the rims run along the zigzag direction of graphene. The plumbene edges are chiral because of the twist, and the appearance of the high intensities at these positions and energies is in agreement with the presence of edge states in the nontrivial band gap of plumbene [20]. Similar observations were made at the step edges of topological crystalline insulators [18].

In summary, we showed that the intercalation of Pb on BL/SiC(0001) results in the formation of twisted plumbene lattices and suspended graphene. At low temperatures, a gap is induced by the proximity-induced modulation of the on site parameters in graphene which explains the metal-insulator transition found in transport [26]. Moreover, the trivial gap of plumbene at E_F was seen in STS, and the element specific transmissions used to receive a depth resolution of the complex heterostructure with STM. We also found evidence for topologically protected edge states along the chiral edges of plumbene at higher positive voltages in agreement with calculations done for plumbene nanostripes [20].

We thank D. Momeni Pakdehi and A. Chatterjee (PTB Braunschweig) for providing us epitaxially grown graphene samples on SiC(0001). This work is supported by the DFG within the Research Unit FOR5242 (Te386/22-1 and Ge1202/15-1).

*christoph.tegenkamp@physik.tu-chemnitz.de

[1] A. K. Geim and K. S. Novoselov, The rise of graphene, Nat. Mater. **6**, 183 (2007).
[2] B. Feng, J. Zhang, Q. Zhong, W. Li, S. Li, H. Li, P. Cheng, S. Meng, L. Chen, and K. Wu, Experimental realization of two-dimensional boron sheets, Nat. Chem. **8**, 563 (2016).
[3] L. Li, S. z. Lu, J. Pan, Z. Qin, Y. q. Wang, Y. Wang, G. y. Cao, S. Du, and H. J. Gao, Buckled germanene formation on Pt(111), Adv. Mater. **26**, 4820 (2014).
[4] F. Reis, G. Li, L. Dudy, M. Bauernfeind, S. Glass, W. Hanke, R. Thomale, J. Schfer, and R. Claessen, Bismuthene on a sic substrate: A candidate for a high-temperature quantum spin hall material, Science **357**, 287 (2017).
[5] M. Švec, P. Hapala, M. Ondráček, P. Merino, M. Blanco-Rey, P. Mutombo, M. Vondráček, Y. Polyak, V. Cháb, J. A. Martín Gago, and P. Jelínek, Silicene versus two-dimensional ordered silicide: Atomic and electronic structure of Si-($\sqrt{19} \times \sqrt{19}$)R23.4°/Pt(111), Phys. Rev. B **89**, 201412 (2014).
[6] L. Zhang, P. Bampoulis, A. N. Rudenko, Q. Yao, A. van Houselt, B. Poelsema, M. I. Katsnelson, and H. J. W. Zandvliet, Structural and Electronic Properties of Germanene on MoS_2, Phys. Rev. Lett. **116**, 256804 (2016).
[7] J. Coraux, A. T. N'Diaye, M. Engler, C. Busse, D. Wall, N. Buckanie, F. J. Meyer zu Heringdorf, R. van Gastel, B. Poelsema, and T. Michely, Growth of graphene on Ir(111), New J. Phys. **11**, 039801 (2009).
[8] K. V. Emtsev, A. Bostwick, K. Horn, J. Jobst, G. L. Kellogg, L. Ley, J. L. McChesney, T. Ohta, S. A. Reshanov, J. Röhrl, E. Rotenberg, A. K. Schmid, D. Waldmann, H. B. Weber, and T. Seyller, Towards wafer-size graphene layers by atmospheric pressure graphitization of silicon carbide, Nat. Mater. **8**, 203 (2009).
[9] Y. Cao, V. Fatemi, S. Fang, K. Watanabe, T. Taniguchi, E. Kaxiras, and P. Jarillo-Herrero, Unconventional superconductivity in magic-angle graphene superlattices, Nature (London) **556**, 43 (2018).
[10] C. Rubio-Verd, S. Turkel, Y. Song, L. Klebl, R. Samajdar, M. S. Scheurer, J. W. F. Venderbos, K. Watanabe, T. Taniguchi, H. Ochoa, L. Xian, D. M. Kennes, R. M. Fernandes, N. Rubio, and A. N. Pasupathy, Moirè nematic phase in twisted double bilayer graphene, Nat. Phys. **18**, 196 (2022).
[11] R. Samajdar, M. S. Scheurer, S. Turkel, C. Rubio-Verd, A. N. Pasupathy, J. W. F. Venderbos, and R. M. Fernandes, Electric-field-tunable electronic nematic order in twisted double-bilayer graphene, 2D Mater. **8**, 034005 (2021).
[12] S. Colonna, R. Flammini, and F. Ronci, Silicene growth on Ag(110) and Ag(111) substrates reconsidered in light of Si-Ag reactivity, Nanotechnology **32**, 152001 (2021).
[13] J. Yuhara and G. Le Lay, Beyond silicene: Synthesis of germanene, stanene and plumbene, Jpn. J. Appl. Phys. **59**, SN0801 (2020).
[14] P. Bampoulis, L. Zhang, A. Safaei, R. van Gastel, B. Poelsema, and H. J. W. Zandvliet, Germanene termination of Ge_2Pt crystals on Ge(110), J. Phys. Condens. Matter **26**, 442001 (2014).
[15] F. f. Zhu, W. j. Chen, Y. Xu, C. l. Gao, D. d. Guan, C. h. Liu, D. Qian, S. C. Zhang, and J. f. Jia, Epitaxial growth of two-dimensional stanene, Nat. Mater. **14**, 1020 (2015).
[16] G. Bihlmayer, J. Sassmannshausen, A. Kubetzka, S. Blügel, K. von Bergmann, and R. Wiesendanger, Plumbene on a Magnetic Substrate: A Combined Scanning Tunneling Microscopy and Density Functional Theory Study, Phys. Rev. Lett. **124**, 126401 (2020).
[17] J. Yuhara, B. He, N. Matsunami, M. Nakatake, and G. Le Lay, Graphene's latest cousin: Plumbene epitaxial growth on a nano watercube, Adv. Mater. **31**, 1901017 (2019).
[18] S. Paolo, D. S. Domenico, S. Andrzej, G. Florian, W. Stefan, S. Henrik, B. Thomas, D. Piotr, G. Martin, N. Titus, S. Giorgio, S. Tomasz, T. Ronny, and B. Matthias, Robust spin-polarized midgap states at step edges of topological crystalline insulators, Science **354**, 1269 (2016).
[19] M. Bauernfeind, J. Erhardt, P. Eck, P. K. Thakur, J. Gabel, T.-N. Lee, J. Schäfer, S. Moser, D. Di Sante, R. Claessen, and G. Sangiovanni, Design and realization of topological

dirac fermions on a triangular lattice, Nat. Commun. **12**, 5396 (2021).
[20] X. L. Yu, L. Huang, and J. Wu, From a normal insulator to a topological insulator in plumbene, Phys. Rev. B **95**, 125113 (2017).
[21] Y. Li, J. Zhang, B. Zhao, Y. Xue, and Z. Yang, Constructive coupling effect of topological states and topological phase transitions in plumbene, Phys. Rev. B **99**, 195402 (2019).
[22] Y. H. Lu, D. Zhou, T. Wang, S. A. Yang, and J. Z. Jiang, Topological properties of atomic lead film with honeycomb structure, Sci. Rep. **6**, 21723 (2016).
[23] S. Mahdavifar, S. F. Shayesteh, and M. B. Tagani, Electronic and mechanical properties of plumbene monolayer: A first-principle study, Physica (Amsterdam) **134E**, 114837 (2021).
[24] C. Riedl, C. Coletti, T. Iwasaki, A. A. Zakharov, and U. Starke, Quasi-Free-Standing Epitaxial Graphene on SiC Obtained by Hydrogen Intercalation, Phys. Rev. Lett. **103**, 246804 (2009).
[25] P. Rosenzweig, H. Karakachian, D. Marchenko, K. Küster, and U. Starke, Overdoping Graphene beyond the van Hove Singularity, Phys. Rev. Lett. **125**, 176403 (2020).
[26] M. Gruschwitz, C. Ghosal, T. H. Shen, S. Wolff, T. Seyller, and C. Tegenkamp, Surface transport properties of Pb-intercalated graphene, Materials **14**, 7706 (2021).
[27] X. Gonze *et al.*, The Abinitproject: Impact, environment and recent developments, Comput. Phys. Commun. **248**, 107042 (2020).
[28] M. Hupalo, J. Schmalian, and M. C. Tringides, "Devil's Staircase" in Pb/Si(111) Ordered Phases, Phys. Rev. Lett. **90**, 216106 (2003).
[29] V. Yeh, M. Yakes, M. Hupalo, and M. C. Tringides, Low temperature formation of numerous phases in Pb/Si(111), Surf. Sci. **562**, L238 (2004).
[30] F. Speck, M. Ostler, J. Röhrl, J. Jobst, D. Waldmann, M. Hundhausen, L. Ley, H. B. Weber, and T. Seyller, Quasi-freestanding graphene on SiC(0001), Mater. Sci. Forum **645–648**, 629 (2010).
[31] B. Matta, P. Rosenzweig, O. Bolkenbaas, K. Küster, and U. Starke, Momentum microscopy of Pb-intercalated graphene on SiC: Charge neutrality and electronic structure of interfacial Pb, Phys. Rev. Research **4**, 023250 (2022).
[32] A. Yurtsever, J. Onoda, T. Iimori, K. Niki, T. Miyamachi, M. Abe, S. Mizuno, S. Tanaka, F. Komori, and Y. Sugimoto, Effects of Pb intercalation on the structural and electronic properties of epitaxial graphene on SiC, Small **12**, 3956 (2016).
[33] Y. Zhang, V. W. Brar, F. Wang, C. Girit, Y. Yayon, M. Panlasigui, A. Zettl, and M. F. Crommie, Giant phonon-induced conductance in scanning tunnelling spectroscopy of gate-tunable graphene, Nat. Phys. **4**, 627 (2008).
[34] F. Calleja, H. Ochoa, M. Garnica, S. Barja, J. J. Navarro, A. Black, M. M. Otrokov, E. V. Chulkov, A. Arnau, A. L. V. de Parga, F. Guinea, and R. Miranda, Spatial variation of a giant spin–orbit effect induces electron confinement in graphene on Pb islands, Nat. Phys. **11**, 43 (2015).